ORIGINAL ARTICLE

Green process of fuel production under porous γ-Al₂O₃ catalyst: Study of activation and deactivation kinetic for MTD process

Yuqin Tian [a,*], Azher M. Abed [b], Aseel M. Aljeboree [c], Halah T. Mohammed [d], Samar Emad Izzat [e], Masoud Habibi Zare [f,*], Hossam Kotb [g], Shaheen M. Sarkar [h]

[a] *Institute of Intelligent Manufacturing, Qingdao Huanghai University, Qingdao, Shandong 266427, China*
[b] *Department of Air Conditioning and Refrigeration, Al-Mustaqbal University College, Babylon, Iraq*
[c] *Chemistry Department, College of Sciences for Women, University of Babylon, Hilla, Iraq*
[d] *Anesthesia Techniques Department, Al-Mustaqbal University College, Babylon, Iraq*
[e] *Pharmacy Department, Al-Nisour University College, Baghdad, Iraq*
[f] *Isfahan University of Technology, Department of Chemical Engineering, 84156-83111 Isfahan, Iran*
[g] *Department of Electrical Power and Machines, Faculty of Engineering, Alexandria University, Alexandria, Egypt*
[h] *Department of Applied Science, Technological University of the Shannon: Midlands Midwest, Moylish, Limerick V94 EC5T, Ireland*

Abstract One of the methods of industrial dimethyl ether production is the catalytic dehydration of methanol. In this research work, methanol dehydration reactor has been modeled using continuous model and its results have been compared with experimental works and Voronoi pore network model. A 1D heterogeneous dispersed plug flow model was utilized to model an adiabatic fixed-bed reactor for the catalytic dehydration of methanol to dimethyl ether. The mass and heat transfer equations are numerically solved for the reactor. The concentration of the reactant and products and also the temperature varies along the reactor, therefore the effectiveness factor would also change in the reactor. We used the the effectiveness factor that was simulated according to the diffusion and reaction in the catalyst pellet as a Voronoi pore network model. Sensitivity analysis was performed to determine the influence of T, P and weight hourly space velocity on performance of the chemical reactor. Acceptable agreement was reached between the measured and the model data. The results showed that the maximum reaction conversion was obtained about 90 % at

* Corresponding authors.
  E-mail addresses: tian1978123@163.com (Y. Tian), masoud.habibi@ce.iut.ac.ir (M.H. Zare).
Peer review under responsibility of King Saud University.

Production and hosting by Elsevier
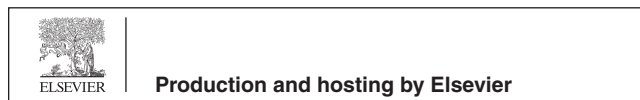
Nomenclature

C	Concentration	U	superficial velocity
C_0	total concentration	x	reactor longitudinal coordinate
c_p	specific heat of fluid	Z	–
d	reactor diameter	α	thermal diffusivity
D_a	dispersion coefficient	ΔH	heat of reaction
$D_{a,k}$	dispersion coefficient	$\Delta \underline{H}$	dimensionless heat of reaction
D_m	molecular diffusion coefficient	ε_{bed}	bed porosity
d_s	particle diameter	$\eta(C_M, T)$	effectiveness factor
K	thermodynamic equilibrium constant	ρ	gas phase density
K_s	reaction rate constant	ρ_B	catalyst bed density
K_M	adsorption constant of methanol	τ_{bed}	tortuosity coefficient
K_w	adsorption constant of water	υ	kinematic viscosity
k_a	axial thermal conductivity	Φ_k^2	thiele modulus
k_p	solids thermal conductivity		
k_f	fluid thermal conductivity		
k_e^0	thermal conductivity of a quiescent bed	*Subscripts*	
L	catalyst bed height	d	DME
Pe_k	Peclet number for k component	k	Methanol, DME
Pe_h	heat Peclet number	M	Methanol
Pr	Prandtle number	W	water
T	temperature		
T_0	inlet temperature		

WHSV = 10 h^{-1} and T = 560 K, while the inlet temperature (T$_{inlet}$) had a greater effect on methanol conversion. In addition, the effect of water in the feed on methanol conversion was quantitatively studied. Also, the deactivation kinetics of γ-Al$_2$O$_3$ heterogeneous-acidic catalyst in methanol to dimethyl ether dehydration process was studied using integral analysis method. Based on independent deactivation kinetics, a second order was found that accurately fitted the experimental conversion time data. The main reaction activation energies and catalyst deactivation energies were 143.1 and −102.1 kJ/mol, respectively.

1. Introduction

Dimethyl ether (DME) is a linear combination, odorless, colorless component and has no corrosive properties. It is also not environmentally hazardous. DME, as a liquefied gas has characteristics similar to those of liquefied petroleum gas (LPG) (Arcoumanis et al., 2008; Semelsberger et al., 2006). It is identified as a potential diesel and cooking fuel. Its oxygen content is 34.78 % and can be burned without soot emission. It has a boiling point of 248 K, which is 293 K higher than LPG and can be liquidized at 5.4 bar (293 K). DME behaves as a gas in standard conditions (0.1 MPa, 298 K) (Semelsberger et al., 2006; Jiang et al., 2021; Li et al., 2021b; Liu, 2008; Mudiyanselage, 2021; Niknam et al., 2021; Pourbavarsad et al., 2021). DME can be produced from a variety of feed-stocks such as natural gas, crude oil, residual oil, coal, waste products and bio-mass (Arcoumanis et al., 2008; Amini et al., 2019; Andalib and Sarkar, 2022; Bakht et al., 2016; Bakhtadze et al., 2020). One of the commercially processes for DME production is the catalytic dehydration of methanol (MeOH). For this reaction, acidic porous catalysts such as zeolites, SiO$_2$–Al$_2$O$_3$, Al$_2$O$_3$ etc. are used (Hassanpour et al., 2010; Keshavarz et al., 2010; Lu et al., 2004; Moradi et al., 2008; Moradi et al., 2008; Yaripour et al., 2005; Yaripour et al., 2009; Hassanpour et al., 2010). The reaction rate for this process is mainly derived under the experimental conditions in the laboratory, while these results are not found in an industrial reactor (Bandiera and Naccache, 1991; Bercic and Levec, 1992; Figueras et al., 1971; Gates and Johanson, 1969; Klusáček and Schneider, 1982). Bercic and Levec reviewed the different reaction rates, and they designed some experiments to study this reaction in industrial conditions using γ-Al$_2$O$_3$ as the catalyst (Bercic and Levec, 1992; Al-Shawi et al., 2021; Alibak et al., 2022; Dong et al., 2020; He et al., 2022; Hutapea et al., 2022; Johnson et al., 2022; Ma et al., 2022). The experimental works were conducted in a differential chemical reactor (8-mm inside diameter) with the temperature variations between 521 and 651 K. Also, in the process, pressure maintained at 1.46 bar. The chemical reactor wroked free of inter particle heat and mass resistances. Bercic and Levec suggested the kinetics of the reaction at this condition (Bercic and Levec, 1992). They also used a laboratory scale reactor to find its conversion and temperature profile in it. Then plug flow condition and longitude changes of concentration and temperature were considered for the reactor modeling. They considered convection and reaction terms in the mass and heat transfer equations. In order to find the effectiveness factor (EF), the continuum model was considered for the spherical catalyst particles. They used a Rang Kutta method to solve the mass and heat transfer equations simultaneously (Bercic and Levec, 1993). Mathematical modeling and kinetics of chemical processes help a lot in simulating any process (Li et al., 2021a; Mianmahale et al., 2021; Kazemeini et al., 2014; Kazemeini et al., 2012). In the modeling presented in this paper we used the results of Voronoi pore network model (VPNM) for the value of EF. In fact, since the catalyst pellet has porous structure, continuum

models cannot predict its behavior precisely (Antoine et al., 2022; Chen et al., 2021a; Chen et al., 2021b; Gao et al., 2022; Huang et al., 2019; Huang et al., 2018; Yin et al., 2022a; Yin et al., 2022b). Any porous structure can be mapped into a VPNM. The pore network models have been extensively used in the last decades. The structure of the porous medium can strongly affect its characteristics (Li et al., 2021c). EF was found based on a three dimensional VPNM for the catalyst pellets (Li et al., 2021c). Here, first the mathematical model was explained, then the mass and heat transfer process were explained in the reactor. Also, the mathematical approach for solving the equations is described as well. After that the results are presented and discussed. In this research work, the MeOH dehydration reactor modeled using the continuous model (CM) was compared with the experimental model and VPNM which was our research work (Li et al., 2021c). In the final part a summary of the paper is presorted. In this work, γ-Al₂O₃ was used as a catalyst for the dehydration of MeOH to DME. We also reached the optimal WHSV, which gives us the maximum MeOH conversion at different MeOH gas inlet temperatures. In the kinetic modeling part of this research work, the "deactivated" rate of γ-Al₂O₃ was modeled in the presence of added water to the MeOH input feed (Shen et al., 2022; Wang et al., 2021; Wang et al., 2020; Wu et al., 2021; Xiong et al., 2020). However, γ-Al₂O₃ catalyst activity was restored after feeding pure MeOH, indicating that activity loss in this catalyst was due to competitive water uptake at active sites. After exposure of the γ-Al₂O₃ catalyst to steam at different T_{inlet}, the conversion of γ-Al₂O₃ to γ-AlO(OH) (Boehmite) was shown to decrease the catalyst activity by about 13 %. However, this conversion was reversible under reaction conditions and γ-AlO(OH) was converted back to γ-Al₂O₃ and recovered the catalyst activity. Fresh and recovered alumina have different textural characteristics, but recovered alumina has a smaller surface area than fresh alumina. However, as far as we know, no kinetic model for catalyst deactivation has been reported in previous research. However, deactivation kinetics are essential for reactor design and predict catalyst lifespan in commercial plants (Sahebdelfar et al., 2022). Also in this research work, a kinetic model for MeOH dehydration to DME and catalyst deactivation on γ-Al₂O₃ catalyst was obtained.

2. Mathematical model

2.1. Model for reaction rate

The dehydration of MeOH is based on the following reversible reaction:

$$2CH_3OH \leftrightarrow C_2H_6O + H_2O \tag{1}$$

The dehydration kinetics of MeOH on acidic catalysts, especially γ-Al₂O₃, have been extensively studied (as shown in Table 1) (Padmanabhan and Eastburn, 1972; Klusáček and Schneider, 1981; Bercic and Levec, 1992; Mollavali et al., 2008; Moradi et al., 2010; Zhang et al., 2011).

To model the production of DME from MeOH dehydration, the Bercic's rate equation has been used in many research works, and the results show that this equation is more widely used and suitable than other proposed equations (Mollavali et al., 2008; Moradi et al., 2010; Fazlollahnejad et al., 2009; Farsi et al., 2010). Also, many kinetic models include conditions to explain the inhibitory effect of water product due to thermodynamic and kinetic factors (ie, competitive absorption at catalyst active sites) (Sahebdelfar et al., 2022).

Based on Table 1; the reaction rate $(-r)$ is considered as follows (Bercic and Levec, 1993):

Table 1 Summary of the published rate equations.

The Rate Equation	Model	Reference
$-r_M = \frac{2r_0 P_M^{1/2}}{P_M^{1/2} + bP_W}$	Padmanabhan	(Padmanabhan and Eastburn, 1972)
$-r_M = \frac{KK_M C_M}{\left(1 + 2\sqrt{K_M C_M} + K_W C_W\right)^2}$	Klusacek and Schneider	(Klusáček and Schneider, 1981)
$-r_M = \frac{KK_M C_M^2}{\left(1 + 2\sqrt{K_M C_M} + K_W C_W\right)^3}$		
$-r_M = \frac{KK_M C_M^2}{\left(1 + 2\sqrt{K_M C_M} + K_W C_W\right)^4}$		
$-r_M = K_s \frac{K_M^2\left(C_M^2 - \frac{C_D C_M}{K}\right)}{\left(1 + 2\sqrt{K_M C_M} + K_W C_W\right)^4}$	Bercic	(Bercic and Levec, 1992)
$-r_M = \frac{K_2 P_M - (K_2/K_{eq})(P_D P_W/P_M)}{K_M P_M + (P_W/K_W) + 1}$	Mollavali	(Mollavali, 2008)
$-r_M = \frac{K_S K_M^2 C_M^2}{(1 + K_M C_M + K_W C_W)^2}$	Moradi	
$-r_M = \frac{K_S K_M^2 C_M^2}{\left(1 + 2(K_M C_M)^{2/3} + K_W C_W\right)^3}$		(Moradi, 2010)
$-r_M = \frac{K_S K_M^2 C_M^2}{\left(1 + 2(K_M C_M)^2 + K_W C_W\right)^4}$		
$-r_M = \frac{kP_M\left(1 - P_W P_D/P_M^2\right)}{\left(1 + 2\sqrt{K_M P_M} + K_W P_W\right)^2}$	Zhang	(Zhang et al., 2011)

P, K and k are partial pressure, equilibrium constant and rate constant of surface reaction respectively,
M, W and D are MeOH, water and DME, respectively.

$$-r = K_s \frac{K_M^2\left(C_M^2 - \frac{C_D C_M}{K}\right)}{\left(1 + 2\sqrt{K_M C_M} + K_W C_W\right)^4} \tag{2}$$

The kinetic constants for MeOH dehydration reaction on γ-Al₂O₃ catalyst are presented in Table 2. The unit of reaction rate calculated using Eq. (2) is $[kmol.(kg_{Catalyst})^{-1}.h^{-1}]$.

2.2. Equilibrium constant

There is not much research to determine the reaction equilibrium constant. Schiffino conducted his research on the equilibrium constant by in the temperature range of 503–623 K using the ideal gas heat capacities and obtained the following expression (T in K) (Schiffino and Merrill, 1993):

$$Ln\ K = -1.7 + \frac{3220}{T} \tag{3}$$

Table 2 The MeOH dehydration reaction kinetic constants on γ-Al₂O₃ catalyst.

Kinetics parameters	Value	Unit
K_S (Bercic and Levec, 1993)	$5.35 \times 10^{13}\exp\left(\frac{-17280}{T}\right)$	$[kmol/kg.hr]$
K_M (Bercic and Levec, 1993)	$5.39 \times 10^{-4}\exp\left(\frac{8487}{T}\right)$	$[m^3/kmol]$
K_W (Bercic and Levec, 1993)	$8.47 \times 10^{-2}\exp\left(\frac{5070}{T}\right)$	$[m^3/kmol]$
K (Schiffino and Merrill, 1993)	$\exp\left(-1.7 + \frac{3220}{T}\right)$	

In another study by Deep and Wainwright, an extensive study of equilibrium conditions in reaction was performed and presented a more general K-to-temperature relationship that is presented elsewhere (Diep and Wainwright, 1987):

$$\ln \ K = \frac{2835.2}{T} - 1.675 \ \ln \ T + 2.39 \times 10^{-4}$$
$$- 0.21 \times 10^{-6} T^2 - 13.36 \tag{4}$$

After two previous research papers, a new relationship has been proposed by H. T. Zhang:

$$\ln \ K = \frac{4019}{T} - 3.707 \ \ln \ T + 2.783 \times 10^{-3} T$$
$$- 3.8 \times 10^{-7} T^2 - 6.561 \times \frac{10^4}{T^3} - 26.64 \tag{5}$$

The schematic diagram of the DME production process cycle by MeOH dehydration method in a catalytic plug reactor from MeOH production from carbon production sources to water and DME production is shown in Fig. 1.

Mathematical modeling for the reactor is built considering: (1) It is operated at steady state conditions; (2) Plug flow is taken into account and the gas phase is assumed to behave ideally; (3) Adiabatic condition is employed, and heat transfer is ignored; (4) The pressure in the reactor is constant. (5) Concentration and temperature changes are considered only in longitudinal direction.

The mass and energy balance equations are arranged according to diffusion, convection and reaction mechanisms in the reactor:

$$\frac{d^2 C_k}{dx^2} - \frac{U}{D_{a,k}} \frac{dC_k}{dx} - \frac{\rho_B v \eta(C_M, T)}{D_{a,k}} (-r) = 0 \tag{6}$$

$$\frac{d^2 T}{dx^2} - \frac{U \rho C_p}{K_a} \frac{dT}{dx} - \frac{\rho_B \Delta H \eta(C_M, T)}{K_a} (-r) = 0 \tag{7}$$

Eq. (6) should be written for MeOH and DME and index k refers to the components. Eqs. (2), (6) and (7) can be changed to a dimensionless form as follows:

$$\frac{d^2 \bar{C}_k}{d\bar{x}^2} - Pe_k \frac{d\bar{C}_k}{d\bar{x}} - \Phi_k^2 v_k \eta(C_M, T)(-R) = 0 \tag{8}$$

$$\frac{d^2 \bar{T}}{d\bar{x}^2} - Pe_h \frac{d\bar{T}}{d\bar{x}} - \bar{\Delta H} \eta(C_M, T)(-R) = 0 \tag{9}$$

$$-R = \frac{K_M^2 C_o^2 \left(\bar{C}_M^2 - \frac{\bar{C}_D \bar{C}_M}{K} \right)}{\left(1 + 2\sqrt{K_M \bar{C}_M} + K_W \bar{C}_W \right)^4} \tag{10}$$

Where $\bar{C} = \frac{C}{C_0}$, $\bar{T} = \frac{T}{T_0}$, $\bar{x} = \frac{x}{L}$. The dimensionless parameters in Eqs. (8) and (9) are:

$$Pe_k = \frac{UL}{D_{a,k}} \tag{11}$$

$$Pe_h = \frac{\rho C_p U L}{K_a} \tag{12}$$

$$\Phi_k^2 = \frac{K_s \rho_B L^2}{D_{a,k} C_0} \tag{13}$$

$$\bar{\Delta H} = \frac{K_s \rho_B L^2 \Delta H}{K_a T_0} \tag{14}$$

The water concentration in each segment can be calculated from the total balance.

$$C_w = C_T - (C_M + C_E) \tag{15}$$

The appearance of EF in Eqs. (8) and (9) is due to the heterogeneity in the reactor and the mass transfer limitation in the catalysts.

We used the results of our previous study to find EF along the reactor (Li et al., 2021c). EF was found based on a three-dimensional VPNM for the catalyst pellets. In that model pores are places where mass transfer and reaction occur, and nodes are interchange points between the pores. For more details, one can refer to the mentioned study where EF is calculated at different temperatures and MeOH concentrations.
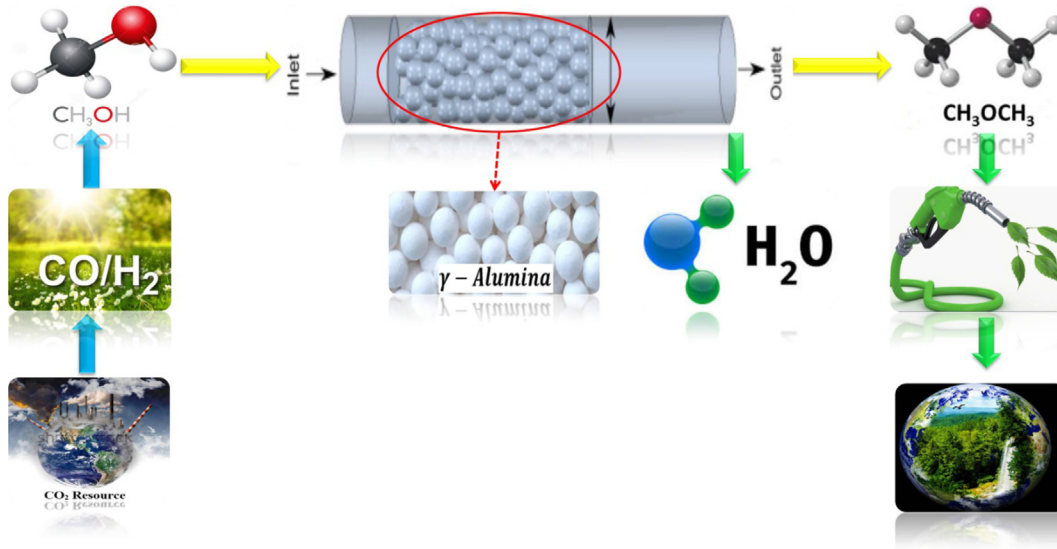

Fig. 1 Schematic diagram of the dimethyl ether production process cycle from carbon production sources (in a catalytic plug reactor).

Eqs. (5) and (6) are solved considering:

$$\bar{x} = 0 \quad \bar{C}_k = \bar{C}_{k,0} \tag{16}$$

$$\bar{x} = 1 \quad \frac{d\bar{C}_k}{d\bar{x}} = 0 \tag{17}$$

$$\bar{x} = 0 \quad \bar{T} = \bar{T}_0 \tag{18}$$

$$\bar{x} = 1 \quad \frac{d\bar{T}}{d\bar{x}} = 0 \tag{19}$$

The dispersion coefficient in Eq. (6) should be considered in the porous packed bed. This parameter is a function of Reynolds number and can be calculated as follows (Berger et al., 2002):

$$\frac{D_a}{\varepsilon_{bed}} = \frac{D_m}{\tau_{bed}} \quad \mathrm{Re} < 1 \tag{20}$$

$$\frac{D_a}{\varepsilon_{bed}} = \frac{D_m}{\tau_{bed}} + 0.5 d_s U \, \mathrm{Re} > 5 \tag{21}$$

The tortuosity in Eqs. (20) and (21) is given by (Epstein, 1989):

$$\tau_{bed} = \frac{1}{\sqrt{\varepsilon_{bed}}} \tag{22}$$

The axial effective thermal conductivity in Eq. (7) is determined by the following equation (Wen and Ding, 2006):

$$\frac{k_a}{k_f} = \frac{k_e^0}{k_f} + 0.5 Re_p Pr \tag{23}$$

where:

$$\frac{k_e^0}{k_f} = \left(\frac{k_p}{k_f}\right)^n \tag{24}$$

where n is:

$$n = 0.28 - 0.757 log(\varepsilon) - 0.057 log\left(\frac{k_p}{k_f}\right) \tag{25}$$

The dimensionless parameters in Eq. (23) are:

$$Re_p = \frac{U d_s}{v} \tag{26}$$

$$Pr = \frac{v}{\alpha} \tag{27}$$

The SRK equation of state is used to calculate the compressibility factor (Prausnitz et al., 1988). Other parameters used in the simulation are presented in Table 3.

The finite difference method is used to solve Eqs. (8) and (9):

$$[2 - Pe_k \Delta x]\bar{C}_{k,i+1} - 4\bar{C}_{k,i} + [2 + Pe_k \Delta x]\bar{C}_{k,i-1} \\ - 2\Delta x^2 \Delta_k^2 v_k \eta(C_M, T)(-R) = 0 \tag{28}$$

$$[2 - Pe_h \Delta x]\bar{T}_{i+1} - 4\bar{T}_i + [2 + Pe_h \Delta x]\bar{T}_{i-1} \\ - 2x^2 \Delta H \eta(C_M, T)(-R) = 0 \tag{29}$$

where k refers to different components (DME and MeOH) and i shows the grid number is Δx the element length in the reactor and here it is considered equal to 0.01 of the reactor length these equation should be written for all the grids. Using the conditions Eqs (16)–(19), the nonlinear set of equations has to be solved in order to calculate the concentration and temperature distributions in the reactor. A try and error method is used to transform the equations into a linear form. Then the set of linear equations is solved using the Lower–Upper (LU) decomposition method. This trial method is repeated until desired precision is obtained.

As shown in Table 4, the reactor process conditions are shown in this research work.

Using Eq's 30 and 31, the reactor performance in terms of conversion (MeOH) and DME selectivity were evaluated:

$$Conversion_{MeOH} = \frac{Q_{MeOH}^{Feed} - Q_{MeOH}^{Outlet}}{Q_{MeOH}^{Feed}} \tag{30}$$

$$Selectivity_{DME} = \frac{2 Q_{DME}^{Outlet}}{Q_{MeOH}^{Feed} - Q_{MeOH}^{Outlet}} \tag{31}$$

In these equations as mentioned, for specific heat capacity (C_{pf}), viscosity (μ) and conductivity (λ_{er}) of the mixture, it is defined as temperature relations. These relationships are based on the mixing and correlation rules of the Perry Handbook of Individual Characteristics of Species as summarized in Tables 5 and 6 (Hayashi and Moffat, 1982).

2.3. Kinetic modeling

In order to analyze the rate-time data, in addition to the deactivation kinetics, a kinetics for the main reaction is needed that can describe the reaction rate in terms of the concentration of reactant species. The result of comparing the kinetics for MeOH dehydration with γ-Al$_2$O$_3$ catalysts showed that simple kinetics based on the power law according to Eq. (32) show a comparable fit with most of the accepted kinetic expressions:

$$-r'_M = K_1 a\left(C_M^2 - \frac{C_D C_W}{K_e}\right) \tag{32}$$

where W, M, and D represent water, MeOH and DME respectively. $-r'_M$ is the dehydration rate of MeOH per catalyst weight, the forward reaction rate constant (k_1), the equilibrium constant at the reaction temperature (K_e), and C_i is concentration of the components. Since there is no volume change in the reaction, Eq. (32) can be written as an equation in terms of the fractional conversion of MeOH, (X_A). (Eq. (33)).

$$-r'_M = \frac{K_1 a C_{M_0}^2}{X_{M_e}}(X_{M_e} - X_M)(X_{M_e} - (2X_{M_e} - 1)X_M) \tag{33}$$

where e and 0 refer to the reactor equilibrium and the input conditions, respectively. The time-dependent catalyst activity (a) is defined as follows:

$$a = \frac{-r'_M(t)}{-r'_M(t = 0)} \tag{34}$$

To deactivate rate an independent decay law in the form of an Eq. (35) is appropriate.

$$-\frac{da}{dt} = k_d a^n \tag{35}$$

Table 3 The used parameters in the simulation.

Parameter	Value	Unit	Parameter	Value	Unit
C_p* (Bercic, 1990)	110	kJ/kmol. K	k_p (Walas, 1985)	0.972	kJ/h.m.K
ΔH_r (Schiffino and Merrill, 1993)	−23.56	kJ/mol	Catalyst Bulk Density, ρ_B (Bercic and Levec, 1993)	882	(kg$_{cat}$ kg$_{cat}$/ m^3
d (Bercic and Levec, 1993)	0.078	m	d_S (Bercic and Levec, 1993)	0.003	m
Catalyst Bed Length, L (Bercic and Levec, 1993)	0.7	m	ρ	0.0825	kmol/m^3 m^3
Catalyst Porosity, ε_{bed} (Bercic and Levec, 1993)	0.4	–	$D_{a,MeOH}$	0.201	m^2/h
$\bar{Z}$(Maloney, 2008)	0.99515	–	$D_{a,DME}$	0.0081	m^2/h
k_a (Walas, 1985)	0.42	kJ/h.m.K	K_f	0.1599	kJ/h.m.K
Catalyst BET Surface Area	183.206	m^2/g$_{cat}$	WHSV**	10	g$_{MeOH}$/g$_{cat}$.h

* The heat capacity used in the modeling was used as a function of temperature (Table 5).
** WHSV used in the modeling was used in the range of 10–150 h^{-1}.

Table 4 The Reactor Process conditions.

Parameter	Value	Unit
MeOH T_{input}	521–651	K
MeOH Volumetric Flow Rate	6.74 and 4.34	L/h
Pressure	2.1	bar
Catalyst	γ − Alumina	–

In this regard, k_d is the deactivation rate constant and n is the deactivation order that should be obtained from the integral analysis of the experimental data. In order to calculate the performance equation of the plug-flow fixed-bed catalystic reactor, the following equation is used.

$$\frac{W}{F_{M_0}} = \frac{\tau'}{C_{M_0}} = \int_0^{X_M} \frac{dX_M}{-r'_M} \tag{36}$$

where the molar flow rate (F_{M_0}) of MeOH, the catalyst charge (W) and τ' is a capacitance coefficient. Substituting Eq. (33) into Eq. (36), Eq (38) is obtained as follows (Sahebdelfar et al., 2022).

$$\tau' = C_{M_0} W / F_{M_0} \tag{37}$$

$$\left(\frac{2k_1 \tau' C_{M_0}(1 - X_{M_e})}{X_{M_e}}\right) = \ln\left(\frac{X_{M_e} - (2X_{M_e} - 1)X_M}{X_{M_e} - X_M}\right) \tag{38}$$

Eq. (38) shows the conversion of MeOH in the absence of catalyst deactivation as a function of operating conditions. MeOH conversion changes with time when the catalyst is deactivated. We determined the dependence of the MeOH conversion-time by solving Eq.s 34, 35, 36 with a initial condition a (t = 0) = 1for Eq. (35). Eq's (39), (40) are obtained for the laws of first- order and second-order decay, respectively (Sahebdelfar et al., 2022).

$$\ln\left(\ln\left(\frac{X_{M_e} - (2X_{M_e} - 1)X_M}{X_{M_e} - X_M}\right)\right)$$
$$= -k_d t + \ln\left(\frac{2k_1 \tau' C_{M_0}(1 - X_{M_e})}{X_{M_e}}\right) \tag{39}$$

$$\frac{\left(\frac{2\tau' C_{M_0}\left(1-X_{M_e}\right)}{X_{M_e}}\right)}{\ln\left(\frac{X_{M_e}-\left(2X_{M_e}-1\right)X_M}{X_{M_e}-X_M}\right)} = \frac{k_d}{k_1} t + \frac{1}{k_1} \tag{40}$$

The results of Eq's 39 or 40 versus time on stream must lead to a straight line of slope and interruption on which k_d and k_1 can be obtained (Sahebdelfar et al., 2022).

3. Results and discussion

3.1. Effect of different conditions on MeOH conversion and reactor temperature

Fig. 2 shows the MeOH concentration versus reactor length. The results are presented for different flow rates and compared to the experimental data. As the flow rate decreases, the residence time will increase and MeOH has more time to be in contact with catalysts in the reactor. Therefore, the equilibrium conversion is achieved in a smaller length from the reactor from the inlet. The mean relative prediction error of the simulation results using continuous and Voronoi models was about 2.11 % and 5.32 %, (q = 6.74 lit/h) and 2.45 % and 7.35 % (q = 4.34 lit/h), respectively.

Fig. 3 presents temperature distribution in the reactor at different flow rates at a constant inlet temperature. Increase in flow rate affects the temperature distribution in the reactor and would decrease it along the reactor. In both flow rates equilibrium condition is attained, and the final temperature

Table 5 Correlation for individual C_P (J/kg.K) = a + bT + cT^2 + dT^3 + eT^4.

Constant	a	b	c	d	e
Water	1914.5	−0.79148	2.6286×10^{-3}	1.98022×10^{-6}	5.1923×10^{-10}
DME	369.68	3.8902	1.1369×10^{-3}	-4.16588×10^{-8}	–
MeOH	660.2	2.2144	8.0777×10^{-4}	-9.0424×10^{-7}	–

Table 6 Correlations of Individual viscosity ($\mu = \frac{C_1 T^{C_2}}{1+C_3/T+C_4/T^4}$) and conductivity ($\lambda = \frac{C_1 T^{C_2}}{1+C_3/T+C_4/T^2}$).

Constant		C_1	C_2	C_3	C_4	Temp. Range(K)
Viscosity	Water	1.7e-6	1.114	–	–	273–1073
	DME	2.6e-6	0.397	534	–	131–1000
	MeOH	3.0e-7	0.696	205	–	240–1000
Conductivity	Water	6.2e-6	1.397	–	–	273–1073
	DME	0.059	0.266	1018.6	1,098,800	248–1500
	MeOH	5.7e-7	1.786	–	–	273–684
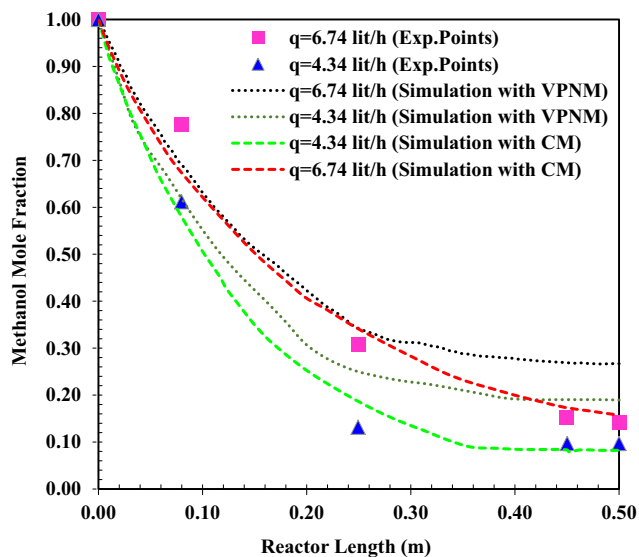
Fig. 2 MeOH mole fraction as a function of reactor length at T_0 = 551 K (VPNM Simulation (Li et al., 2021c), (Exp.Points (Bercic and Levec, 1993).
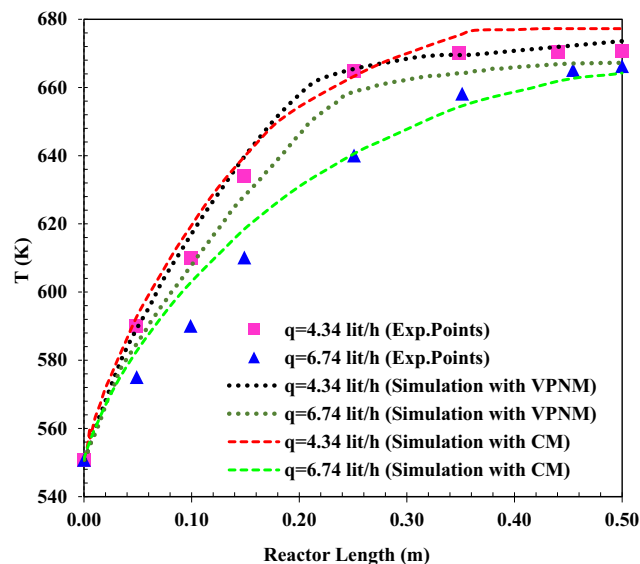
Fig. 3 The simulated reactor temperature as a function of reactor length at T_0 = 551 K (VPNM Simulation (Li et al., 2021c), ((Exp.Points (Bercic and Levec, 1993)).

is the same. However, when the flow rate decreases the final temperature occurs at a distance closer to the reactor inlet. The mean relative prediction error of the simulation results using continuous and Voronoi models was about 3.88 % and 1.13 %, (q = 4.34 lit/h) and 2.93 % and 6.95 % (q = 6.74 lit/h), respectively.

The effect of increase in T_{inlet} on MeOH concentration distribution in the reactor is demonstrated in Fig. 4 As the T_{inlet} increases, the reaction rate would also increase, and the equilibrium conversion is attained in a smaller length of the reactor. Therefore, the upper limit of the temperature corresponding to the equilibrium condition is closer to the reactor inlet (Li et al., 2021c). The mean relative prediction error of the simulation results using continuous and Voronoi models was about 11.64 % and 3.77 %, (T = 551 K) and 9.78 % and 3.58 % (T = 561 K), respectively.

The effect of T_{inlet} on temperature distribution in the fixed-bed catalytic reactor is also shown in Fig. 5. Higher T_{inlet} would increase the reaction rate and therefore the temperature would also be higher along the reactor. The final temperature due to equilibrium condition happens closer to the reactor inlet consequently (Li et al., 2021c). The mean relative prediction error of the simulation results using continuous and Voronoi

models was about 14.88 % and 8.93 %, (T = 551 K) and 23.45 % and 8.33 % (T = 561 K), respectively.

Fig. 6 presents the concentration distribution of DME, MeOH and water along the reactor. As expected DME Concentration increase along the reactor while MeOH decreases.

The effect of inlet MeOH concentration on concentration distribution in the reactor is studied in Fig. 7 If MeOH includes some water at the reactor inlet, DME conversion would strongly reduce. The MeOH concentration along the reactor would be higher or in other words the DME concentration would be less as the inlet water. Content of MeOH increases and the necessary reactor length would increase. Therefore feed water content affects reactor length (Li et al., 2021c).

As shown in Fig. 8, the results of the experimental work; VPNM and the continuous model are compared with each other. Comparing the results of the two methods shows that both models predict the same results for the MeOH concentration and temperature distributions throughout the reactor. Due to the simplicity of the continuous model for predicting the behavior of the reactor, this method is superior to the Voronoi pore network method. The average standard deviation
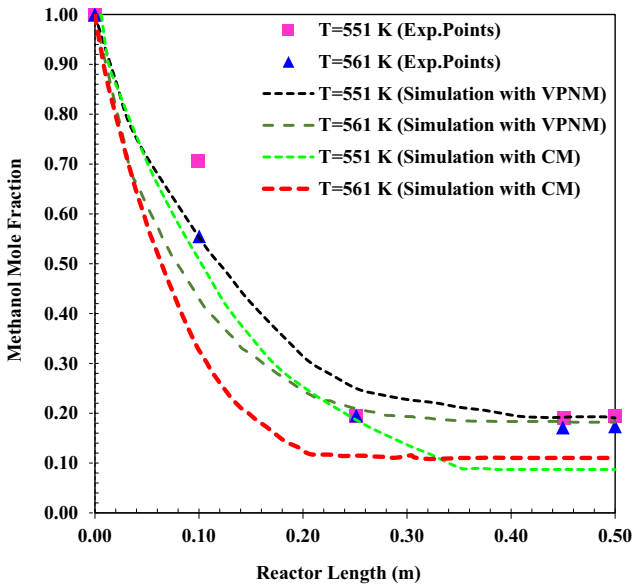
Fig. 4 MeOH mole fraction as a function of reactor length at different inlet temperature (VPNM Simulation (Li et al., 2021c), (Exp.Points (Bercic and Levec, 1993).
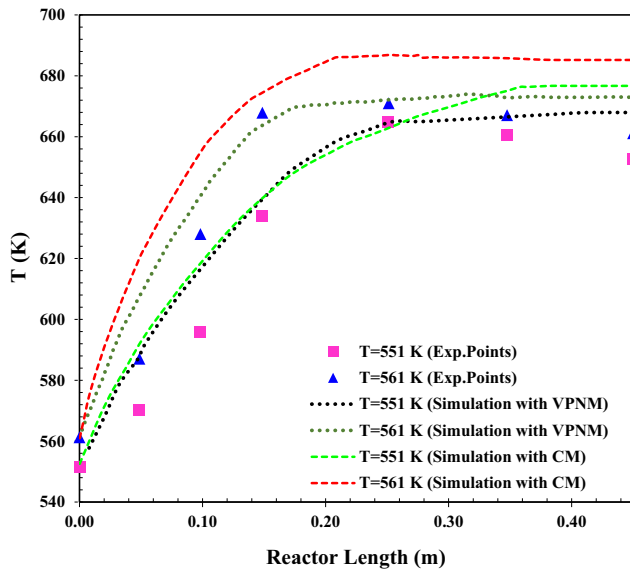

Fig. 5 The simulated reactor temperature as a function of reactor length at different inlet temperature (VPNM Simulation (Li et al., 2021c), (Exp.Points (Bercic and Levec, 1993).

Fig. 6 MeOH and DME mole fraction as a function of reactor length at q = 4.34 L/h and at T_0 = 551 K. (VPNM Simulation (Li et al., 2021c),
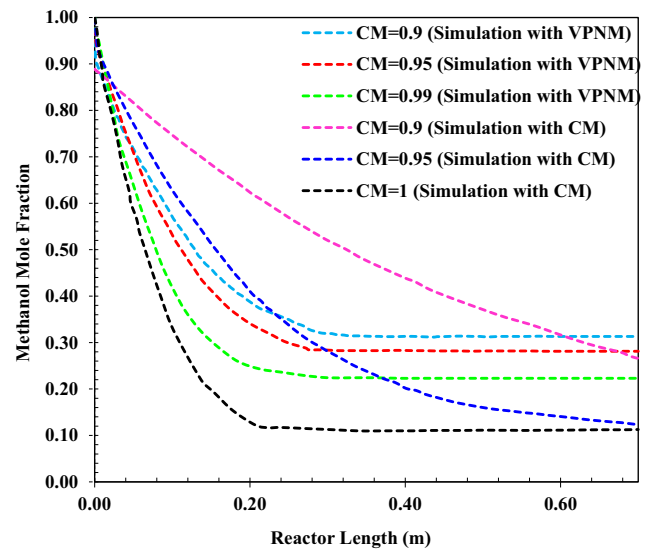

Fig. 7 MeOH mole fraction as a function of reactor length at q = 4.34 L/h and at T_0 = 561 K for different CM. (VPNM Simulation (Li et al., 2021c).

for Voronoi and continuous models is 19 % and 28 %, respectively, which is desirable for present modeling.

3.2. The equilibrium conversion of MeOH

The equilibrium conversion results of MeOH by experimental models along with the continuous model are shown in Fig. 9. These results show that for exothermic reactions, with increasing temperature has a negative effect. Because this reaction is reversible, the equilibrium conversion of MeOH also decreases with increasing temperature. Approximately T = 520 to 651 K

can be considered as the best temperature range for the process (Li et al., 2021c).

Equilibrium conversions are calculated from the previously relationships and by showing the experimental data to each other, the best fixed equilibrium model is obtained. It is clear from Fig. 8 that our correlations and the correlations proposed by Bercic and Levec with experimental data are higher than other correlations (Li et al., 2021c).

Based on Bercic rate and continuous and Voronoi Pore Network models, the simulations were confirmed in comparison with the experimental data and the results are shown in Fig. 10. The mean relative prediction error of the simulation results using continuous and Voronoi models was about 4.61 % and 11.12 %, respectively.
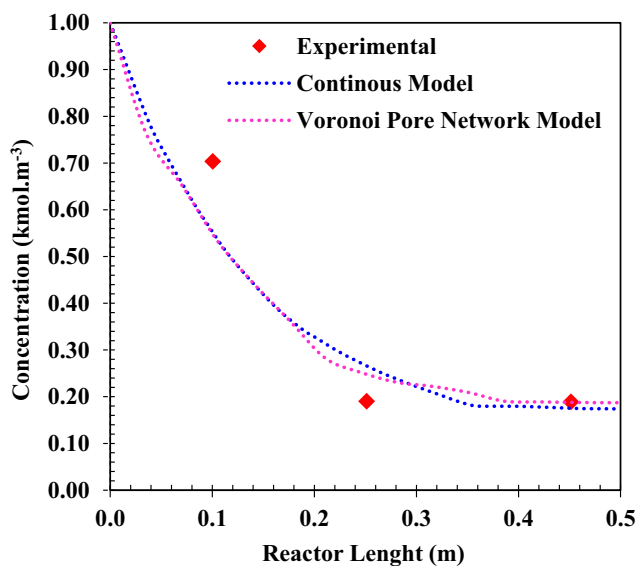
Fig. 8 Comparison of MeOH concentration distributions from experimental work (Bercic and Levec, 1993); Voronoi pore network (Li et al., 2021c) and continuous models.
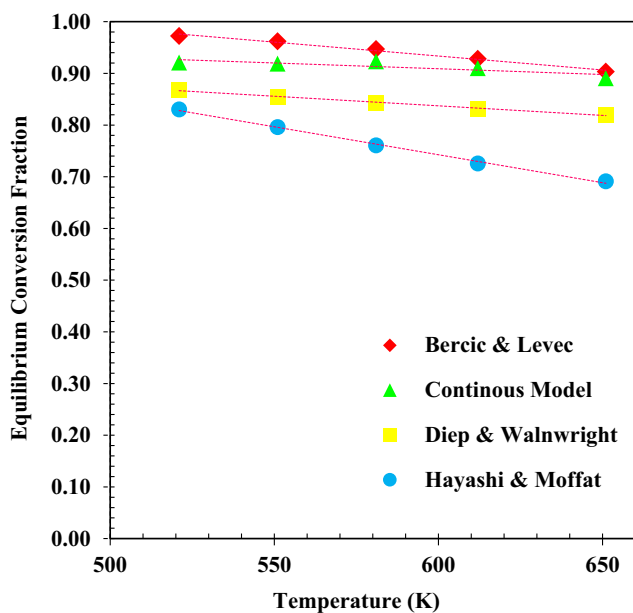

Fig. 9 MeOH equilibrium conversion (Experimental Data (Bercic and Levec, 1992; Bercic, 1990; Ortega et al., 2018) versus temperature.

It can be argued that two mechanisms are simultaneously possible for the production of DME in MeOH dehydration. The mechanism of separation of the two molecules of MeOH is predominant above 551 K and the other mechanism is more common at temperatures below 551 K. The Bercic rate equation was obtained in the temperature range of 521–651 K. The distance shown in Fig. 10 is about 551 K. In addition, the Bercic rate equation and the continuous model perform well for the high temperatures shown in Fig. 10. Selectivity for the production of DME under different T_{inlet} and MeOH
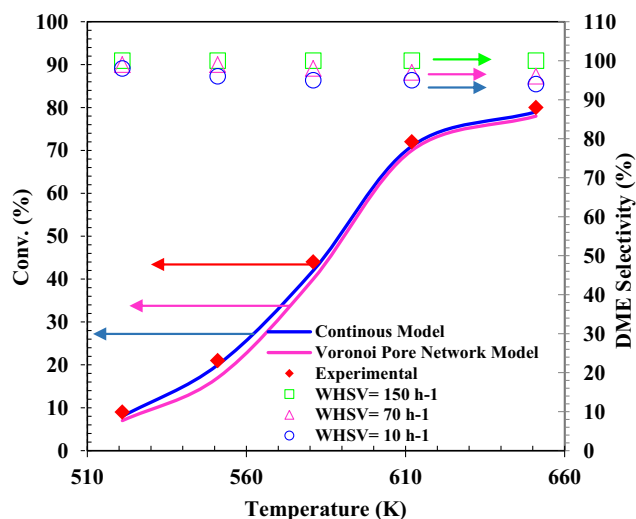

Fig. 10 Comparison of MeOH conversion-temperature results obtained from continuous and Voronoi Pore Network models versus experimental results and DME selectivity (%) at different T_{inlet} and WHSV.

space velocities is shown in Fig. 10. As expected, the MeOH conversion increased with increasing reaction temperature, reaching a maximum at 651 K, while process selectivity relative to DME for different space velocities in the T_{inlet} range of 521–651 K remains an almost constant value of 100 %, with the difference that in the amount of lower space velocity, less selectivity was obtained, also increasing the T_{inlet} is a negative parameter on selectivity. The results confirm the good performance of γ-Al₂O₃ catalyst in the reaction of DME production from MeOH dehydration.

3.3. Effect of pressure on MeOH conversion

According to Le Chatelier principle, pressure change only affects equilibrium systems if the number of moles of the reactant and product gases on both sides of the balanced chemical equation is not the same. On the other hand, the effect of pressure on equilibrium in systems that are only solid, or liquid is minor. Therefore, it is ignored. As shown in Fig. 11, pressure does not affect the conversion of MeOH, and hence the key operational parameters are the temperature and weight hourly space velocity (WHSV). The temperature and WHSV effects on MeOH conversion for WHSV = 10–150 h⁻¹ and T_{inlet} = 521 to 651 K have been investigated.

3.4. Effect of T_{inlet} on MeOH conversion

The effect of T_{inlet} on MeOH conversion in the range of 521–621 K in different WHSV's is shown in Fig. 11. As shown in this figure, MeOH conversion increases with increasing temperature, fastest increase in conversion vs T_{inlet} is observed at WHSV values of 10 and 30 h⁻¹, where MeOH conversion achieves equilibrium conversions due to the slow reactants. Because the equilibrium conversion of an exothermic reaction decreases with increasing temperature, the conversion at WHSV also decreases by 10 and 30 h⁻¹. Also, MeOH conversion in a fixed bed catalytic reactor must operate at the lowest
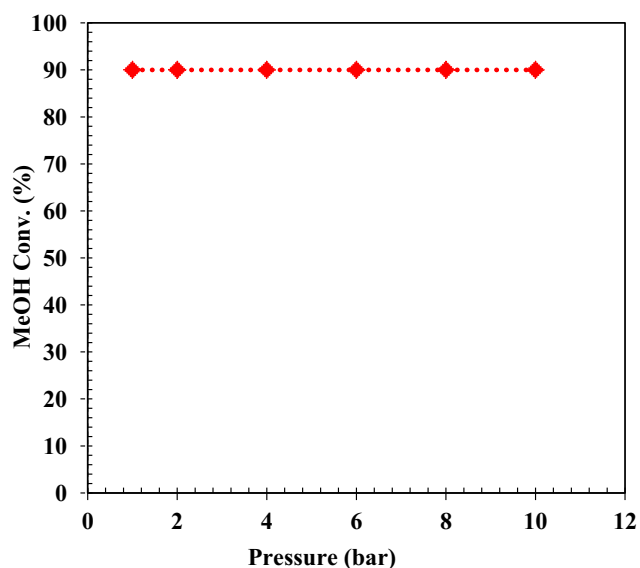
Fig. 11 Effect of pressure on MeOH conversion (Based on rate equations Ref. (Mollavali, 2008).

possible T_{inlet} to benefit the system thermodynamics. This reduction in T_{inlet} makes it possible to use a plug reactor, which is almost impossible at normal inlet temperatures (651 K) because the boiling water pressure rises about 200 bar and makes the reactor very expensive.

According to Fig. 12, at WHSV = 10 h^{-1} and at 560 K, a maximum conversion of 90 % is achieved. This means that the best conditions occurred at the minimum WHSV value at moderate temperatures. Fig. 12 shows that the temperature effect on MeOH conversion is much greater than that of WHSV. As expected, lower T_{inlet} and higher WHSV's decrease the possibility of external mass transfer resistances and limitations. The calculated and equilibrium conversion of MeOH converged at temperature = about 610 K and then both slowly decreased with increasing temperature due to thermodynamic constraints. At temperatures below 610 K, the reaction was kinetically controlled under the given operating conditions.
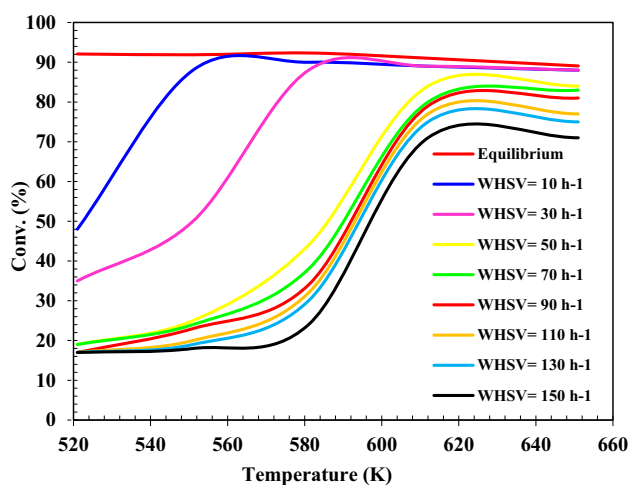
3.5. Effect of WHSV on MeOH conversion

The effect of WHSV on MeOH conversion in the range of 10–160 h^{-1} under different T_{inlet} is also shown in Fig. 13. The results show a decrease in MeOH conversion. At 651 K, the conversion reaction is a weak function of WHSV. At constant T_{inlet}, MeOH conversion increases with decreasing WHSV. Increasing WHSV increases the gas velocity, which increases mass transfer in the system. Also, in higher WHSV the operating temperature must be increased to have a better MeOH conversion. Reactions at temperatures higher 581 K and WHSV lower than 60 h^{-1} led to almost maximum conversion and mass transfer limited conditions.

3.6. Effect of inlet water content on MeOH conversion

The effect of inlet water content on the MeOH conversion reaction was shown in Fig. 14. This effect was investigated at three levels of water mass fraction, i.e., 0.05, 0.1 and 0.5, in the input feed and in the temperature range of 521–651 K and in the WHSV = 50 and 130 h^{-1}. The presence of water at the reactor inlet has a negative effect on MeOH conversion because water is the product of the reaction and according to Le Chatelier principle, the rate of direct reaction is reduced under these conditions. The increase in feed water content reduces the MeOH equilibrium conversion that can be attained, since it favors the reversible reaction (DME + H_2O → MeOH). As the temperature increases, the equilibrium conversion suffers a further decrease and this is caused by the reduction of the equilibrium constant with an increase in temperature (Osman and Abu-Dahrieh, 2018).

3.7. Activation and deactivation kinetic of γ-Al_2O_3 catalyst

The values for the kinetics parameters for the first- and second-order decay laws under different temperature conditions are shown in Table 7. Kinetic parameters were obtained using regression analysis by "Linest function". Also, the results of
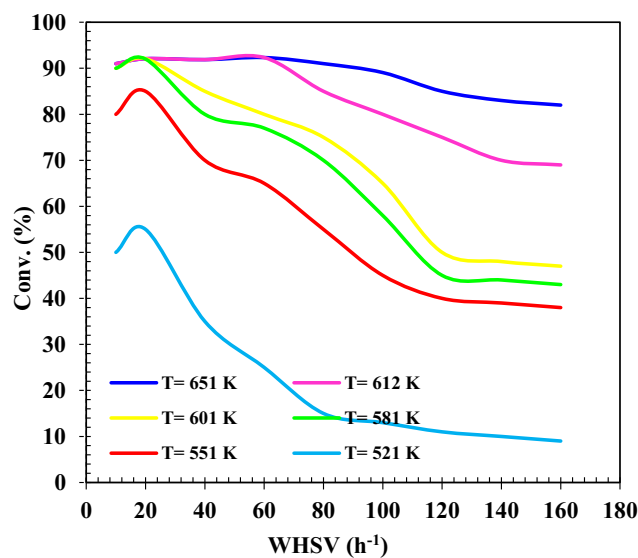

Fig. 12 Conversion of MeOH dehydration reaction (%) at different T_{inlet} and WHSV.

Fig. 13 Conversion of MeOH (%) versus different WHSV and different T_{inlet}.
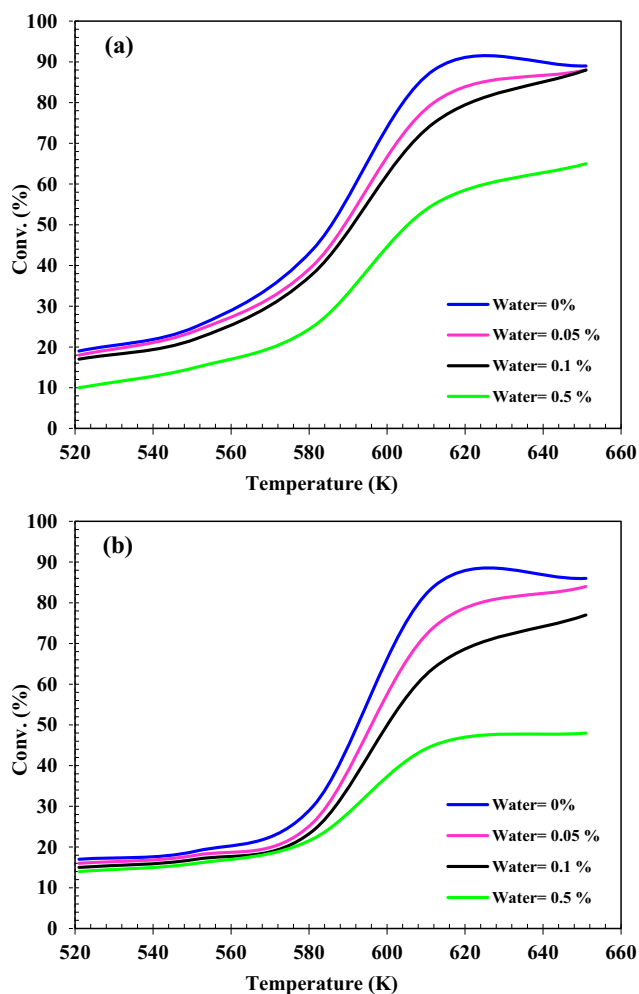
Fig. 14 MeOH conversion versus T_{inlet} under water mass fraction different conditions at (a) WHSV = 50 h^{-1}; (b) WHSV = 130 h^{-1}.
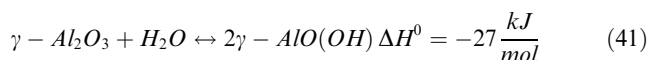
activation energy (E_a) and pre-exponential factor obtained from the kinetic parameters. As can be seen from the kinetic parameter values in Table 7, the values of the deactivation rate constants based on both decays at the same reaction temperature show a larger difference than the numerical values of the main reaction rate constants due to the difference in functionality in the decay laws.

In order to estimate the reaction E_a and catalyst deactivation, Arrhenius plots were shown according to the first- and second-order decay laws of MeOH dehydration rate constants as shown in Fig. 15. The obtained straight lines from results in the Arrhenius plots are logical. The slope and intercept obtained from the Arrhenius plots were used to calculate the E_a and PFE, respectively. The calculated values of the main reaction E_a based on the first and second order decay kinetics determined from Fig. 15 were obtained as 140.33 ± 9.21 kJ/mol and 143.1 ± 9.21 kJ/mol, respectively, which is in good agreement with the values obtained by previous studies (Bercic and Levec, 1992; Panasyuk et al., 2015).

Activation energies for γ-Al₂O₃ catalyst deactivation according to Fig. 16 were obtained based on first- and second-order decay kinetics of −96.49 ± 4.3 and −102.16 ± 4.4 kJ/mol, respectively. The results of both first- and second-order decay laws show negative activation energies for γ-Al₂O₃ catalyst decay. Negative E_a for catalyst deactivation indicates that the γ-Al₂O₃ catalyst deactivation rate decreases with increasing reaction temperature. Negative E_a (<0) suggests that the permeance of the component decreases with temperature.

When the overall reaction rate or deactivation is limited by an exothermic reversible process such as adsorption under reaction conditions, the reaction rate usually decreases as the temperature increase (In multi-step reactions). The steam resulting from the conversion of MeOH to DME can act as a temporary poison to block the catalyst active sites by converting γ-Al₂O₃ to γ-AlO(OH) less catalyst active (based on (41)) (Boon et al., 2019):

$$\gamma - Al_2O_3 + H_2O \leftrightarrow 2\gamma - AlO(OH) \quad \Delta H^0 = -27 \frac{kJ}{mol} \quad (41)$$

The conversion of γ-Al₂O₃ to γ-AlO(OH) occurs at 523 K and high partial vapor pressure (Zhang et al., 2011). The deactivation reaction of the γ-Al₂O₃ catalyst is exothermic, which can be reversed at temperatures above 773 K. therefore, the apparent E_a includes the intrinsic E_a and the adsorption enthalpy term, which may predominate over the former.

Table 7 The values for the kinetics parameters for decay laws under different temperature conditions, E_a and PEF obtained for γ-Al₂O₃ catalyst.

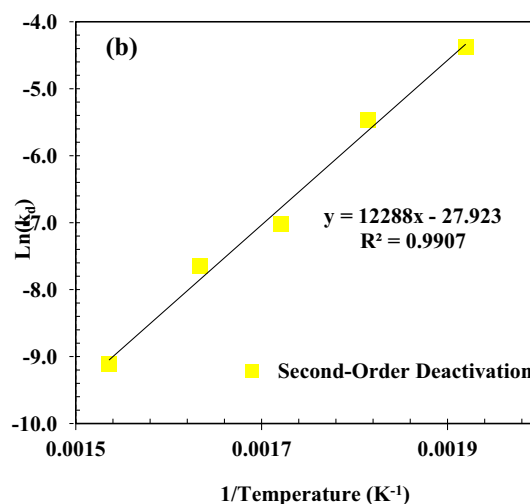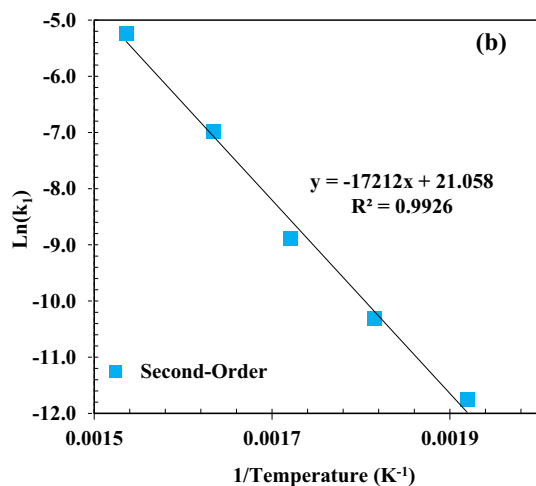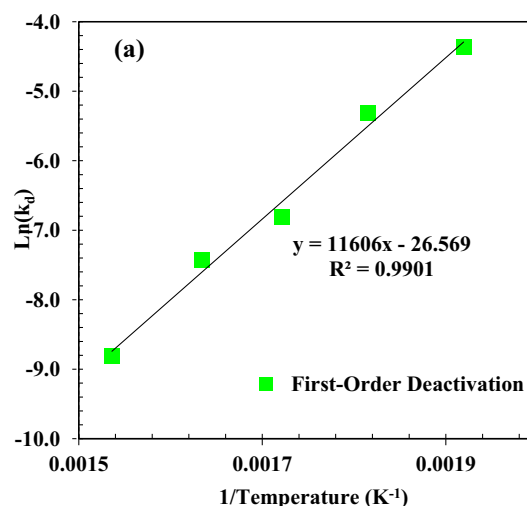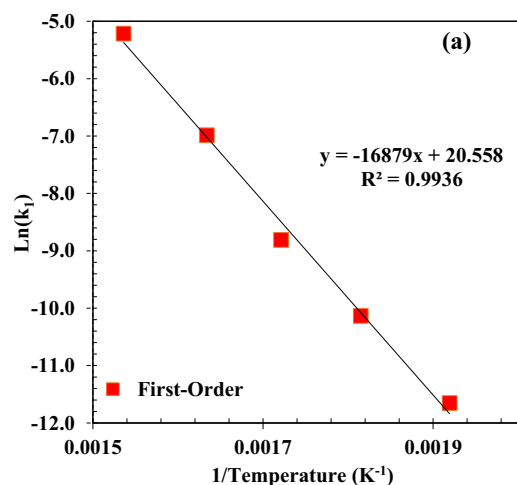| Temperature (°C)	WHSV (h^{-1})	First-Order Deactivation		Second-Order Deactivation	
		k_1 [m^6.mol^{-1}.g$_{cat}^{-1}$.min^{-1}]	k_d [h^{-1}]	k_1 [m^6.mol^{-1}.g$_{cat}^{-1}$.min^{-1}]	k_d [h^{-1}]
521	10	0.0000087	0.0127	0.0000079	0.0125
551	10	0.0000397	0.0049	0.0000333	0.0042
581	30	0.000149	0.0011	0.000138	0.0009
612	70	0.000924	0.00059	0.00092	0.00048
651	70	0.00543	0.00015	0.00532	0.00011
Catalyst		**Activation Energy (kJ/mol)**	**PEF***	**Activation Energy (kJ/mol)**	**PEF**
γ-Al₂O₃		140.33 ± 9.21	−96.49 ± 4.3	143.1 ± 9.21	−102.6 ± 4.4

* Pre-Exponential Factor.

Fig. 15 Arrhenius plot of rate constants against temperature for MeOH dehydration considering with decay law of (a) first-order and (b) second-order.

Fig. 16 Arrhenius plot for deactivation rate constants of MeOH dehydration considering with decay law of (a) first-order (b) second-order.

3.8. γ-Al$_2$O$_3$ catalyst deactivation mechanism

In the stability test under reaction conditions, the activity of the catalyst was measured for a period of 100 h on stream, to detect signs of catalyst deactivation (Fig. 17). Conversion of MeOH (x_M) was used as an indicator of the γ-Al$_2$O$_3$ catalyst performance. The process condition was considered at $T_{inlet} = 551$, 581 and 651 K, feeding MeOH at a WHSV = 20 h^{-1}. The catalyst activity must remain constant. As a result of MeOH conversion, a drop of approximately 13 % was shown, followed by a 2 % relative recovery after steaming, followed by a slow decreasing trend. The results obtained from the γ-Al$_2$O$_3$ catalyst deactivation mechanism model ensure the stability of the catalyst activity under 400 h of kinetic test. During the reaction, the catalyst is deactivated due to the formation of coke, and this deactivation of γ-Al$_2$O$_3$ catalyst leads to a decrease in MeOH conversion over time. The activity of the γ-Al$_2$O$_3$ catalyst should not change or even improve with steaming if the cause of the catalyst deactivation is due to
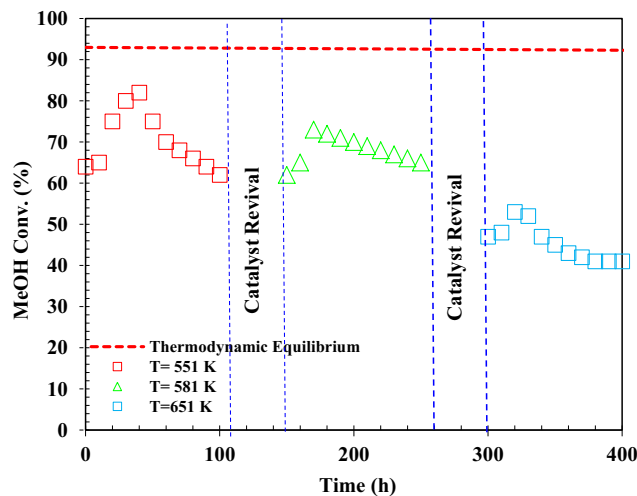

Fig. 17 Effect of steaming on the catalyst activation under different $T_{inlet} = 551$, 581 and 651 K and WHSV = 20 h^{-1}.

the formation of coke because steam is a coke removal agent. As the results show, the reduction in MeOH conversion must be mainly due to γ-Al$_2$O$_3$ conversion to γ-AlO(OH) by steam.

4. Conclusion

Modeling and simulation for the MeOH dehydration process is studied. The effectiveness factor is considered due to VPNM results for catalyst pellets. The simulations indicate that MeOH T_{inlet} and its flow rate affect concentration and temperature distribution in the reactor. Increase in T_{inlet} and decrease in MeOH flow rate causes the equilibrium condition occur in a smaller length from the reactor inlet. The presence of water in the inlet MeOH would decrease the reaction rate in the reactor as well. As can be seen from the results of the two models selected to model the MeOH dehydration reactor, both models modeled the reactor well. The continuous model is proposed due to its simplicity for modeling the MeOH hydration reactor and the VPNM will give better results for the reaction conditions with a very porous catalyst bed. The Bercic model has the best MeOH conversion prediction among all the rate equations listed in Table 1. The Bercic rate equation predicted the MeOH conversion model with an average error of 14 %. The process of producing DME from MeOH dehydration was simulated in the temperature range of about 521–651 K and space velocity in the range of 10 to 150 h^{-1}. Maximum MeOH conversion in reaction conditions in the temperature range was 521 to 651 K and at WHSV = 10 h^{-1} with MeOH conversion 83 to 85 %; The best conditions for the conversion process of MeOH to DME in WHSV = 10 h^{-1}, T was obtained = 563.15 K, and MeOH conversion = 85.03 %. Also, in order to obtain MeOH conversion, the process conditions are presented in two states of pure MeOH input feed and MeOH input feed with water presence. The results of the presence of water, along with MeOH feed, showed a negative effect of water as a reactive. The results showed that MeOH T_{inlet} is the main factor controller of the concentration and profile of temperature as well as MeOH conversion in this process. Also, these results showed that at temperatures above 583.15 K, space velocity had a minor effect on MeOH conversion. It is concluded that the negative effect of increasing space velocity can be compensated by increasing temperature. The study of γ-Al$_2$O$_3$ deactivation kinetics in the reaction of DME production by MeOH dehydration is difficult due to its very slow rate. The low decay rates obtained for γ-Al$_2$O$_3$ catalyst cause uncertainty in calculating the kinetic parameters of catalyst deactivation unless long enough times are used to achieve significant catalyst deactivation. In the present work, the main deactivation mechanisms of of γ-alumina catalyst, including MeOH chemical conversion, coking and sintering, may be predominant depending on the reaction conditions of the MeOH conversion to DME. Therefore, modeling catalyst deactivation experiments is very difficult because the mechanism of catalyst deactivation and its kinetics are only applicable to industrial operating conditions. The present kinetic modeling provides an excellent insight into the deactivation kinetic of γ-Al$_2$O$_3$ catalyst in MeOH dehydration to DME and related kinetic parameters. Advanced kinetic models can be used to accurately predict the main reaction deactivation kinetics which requires more complex solution methods, longer computational times, more accurate data, and much more. However, such calculations are appropriate given the future work in this area.

Declaration of Competing Interest

The authors declare that they have no known competing financial interests or personal relationships that could have appeared to influence the work reported in this paper.

References

Alibak, A.H. et al, 2022. Simulation the adsorption capacity of polyvinyl alcohol/carboxymethyl cellulose based hydrogels towards methylene blue in aqueous solutions using cascade correlation neural network (CCNN) technique. J. Cleaner Prod. 337, 130509.

Al-Shawi, S.G. et al, 2021. Synthesis of NiO Nanoparticles and Sulfur, and Nitrogen co Doped-Graphene Quantum Dots/ NiO Nanocomposites for Antibacterial Application. J. Nanostruct. 11 (1), 181–188.

Amini, S.M., Osanloo, M., Sedaghat, M.M., 2019. Larvicidal activity of chemically synthesized silver nanoparticles against Anopheles stephensi. J. Pharmaceut. Negative Results 10, 69–74.

Andalib, V., Sarkar, J., 2022. A System with Two Spare Units, Two Repair Facilities, and Two Types of Repairers. Mathematics 10 (6), 852.

Antoine, D. et al, 2022. Rapid, Point-of-Care scFv-SERS Assay for Femtogram Level Detection of SARS-CoV-2. ACS Sensors 7 (3), 866–873.

Arcoumanis, C. et al, 2008. The potential of di-methyl ether (DME) as an alternative fuel for compression-ignition engines: A review. Fuel 87 (7), 1014–1030.

Bakht, M.A. et al, 2016. Physicochemical characterization of benzalkonium chloride and urea based deep eutectic solvent (DES): A novel catalyst for the efficient synthesis of isoxazolines under ultrasonic irradiation. J. Mol. Liq. 224, 1249–1255.

Bakhtadze, V. et al, 2020. Activity of Pd-MnOx/Cordierite (Mg, Fe) 2Al4Si5O18) catalyst for carbon monoxide oxidation. Eur. Chem. Bull. 9, 75.

Bandiera, J., Naccache, C., 1991. Kinetics of methanol dehydration on dealuminated H-mordenite: Model with acid and basic active centres. Appl. Catal. 69 (1), 139–148.

Bercic, G., 1990. Dehydration of methanol over gamma alumina kinetics of reaction and mathematical model of an industrial reactor. the University of Ljubljana.

Bercic, G., Levec, J., 1992. Intrinsic and global reaction rate of methanol dehydration over. gamma.-alumina pellets. Ind. Eng. Chem. Res. 31 (4), 1035–1040.

Bercic, G., Levec, J., 1992. Intrinsic and global reaction rate of methanol dehydration over.gamma.-alumina pellets. Ind. Eng. Chem. Res. 31 (4), 1035–1040.

Bercic, G., Levec, J., 1993. Catalytic dehydration of methanol to dimethyl ether. Kinetic investigation and reactor simulation. Ind. Eng. Chem. Res. 32 (11), 2478–2484.

Berger, R.J. et al, 2002. Catalyst performance testing: Radial and axial dispersion related to dilution in fixed-bed laboratory reactors. Appl. Catal. A 227 (1), 321–333.

Boon, J. et al, 2019. Reversible deactivation of γ-alumina by steam in the gas-phase dehydration of methanol to dimethyl ether. Catal. Commun. 119, 22–27.

Chen, T.-C. et al, 2021a. Engineering of Novel Fe-Based Bulk Metallic Glasses Using a Machine Learning-Based Approach. Arabian J. Sci. Eng. 46 (12), 12417–12425.

Chen, T.-C. et al, 2021b. Application of machine learning in rapid analysis of solder joint geometry and type on thermomechanical useful lifetime of electronic components. Mech. Adv. Mater. Struct., 1–9

Diep, B.T., Wainwright, M.S., 1987. Thermodynamic equilibrium constants for the methanol-dimethyl ether-water system. J. Chem. Eng. Data 32 (3), 330–333.

Dong, H. et al, 2020. Characterization and Application of Lignin-Carbohydrate Complexes from Lignocellulosic Materials as Antioxidants for Scavenging In Vitro and In Vivo Reactive Oxygen Species. ACS Sustainable Chem. Eng. 8 (1), 256–266.

Epstein, N., 1989. On tortuosity and the tortuosity factor in flow and diffusion through porous media. Chem. Eng. Sci. 44 (3), 777–779.

Farsi, M., Jahanmiri, A., Eslamloueyan, R., 2010. Modeling and optimization of MeOH to DME in isothermal fixed-bed reactor. Int. J. Chem. Reactor Eng. 8 (1).

Fazlollahnejad, M. et al, 2009. Experimental study and modeling of an adiabatic fixed-bed reactor for methanol dehydration to dimethyl ether. Chin. J. Chem. Eng. 17 (4), 630–634.

Figueras, F. et al, 1971. Dehydration of methanol and tert-butyl alcohol on silica-alumina. Trans. Faraday Soc. 67, 1155–1163.

Gao, N. et al, 2022. Acoustic Metamaterials for Noise Reduction: A Review. Adv. Mater. Technol. 7 (6), 2100698.

Gates, B.C., Johanson, L.N., 1969. The dehydration of methanol and ethanol catalyzed by polystyrene sulfonate resins. J. Catal. 14 (1), 69–76.

Hassanpour, S., Taghizadeh, M., Yaripour, F., 2010. Preparation, Characterization, and Activity Evaluation of H-ZSM-5 Catalysts in Vapor-Phase Methanol Dehydration to Dimethyl Ether. Ind. Eng. Chem. Res. 49 (9), 4063–4069.

Hassanpour, S., Yaripour, F., Taghizadeh, M., 2010. Performance of modified H-ZSM-5 zeolite for dehydration of methanol to dimethyl ether. Fuel Process. Technol. 91 (10), 1212–1221.

Hayashi, H., Moffat, J., 1982. The properties of heteropoly acids and the conversion of methanol to hydrocarbons. J. Catal. 77 (2), 473–484.

He, H. et al, 2022. Metal–organic framework supported Au nanoparticles with organosilicone coating for high-efficiency electrocatalytic N2 reduction to NH3. Appl. Catal. B 302, 120840.

Huang, C. et al, 2018. Unveiling the Structural Properties of Lignin-Carbohydrate Complexes in Bamboo Residues and Its Functionality as Antioxidants and Immunostimulants. ACS Sustainable Chem. Eng. 6 (9), 12522–12531.

Huang, C. et al, 2019. Revealing the effects of centuries of ageing on the chemical structural features of lignin in archaeological fir woods. New J. Chem. 43 (8), 3520–3528.

Hutapea, S. et al, 2022. Study on food preservation materials based on nano-particle reagents. Food Sci. Technol. (Campinas) 22, e39721.

Jiang, J., Zhang, T., Chen, D., 2021. Analysis, Design, and Implementation of a Differential Power Processing DMPPT With Multiple Buck-Boost Choppers for Photovoltaic Module. IEEE Trans. Power Electron. 36 (9), 10214–10223.

Johnson, J., Shanmugam, R., Thangavelu, L., 2022. A Review on plant mediated selenium nanoparticles and its applications. J. Popul. Therapeut. Clin. Pharmacol. 28, e29–e40.

Kazemeini, M. et al, 2012. Theoretical investigations of methane conversion to heavier hydrocarbons in a plasma reactor. Advanced Materials Research. Trans Tech Publ..

Kazemeini, M., Zare, M.H., Fattahi, M., 2014. Mathematical modelling of the methane conversion to heavier hydrocarbons in a plasma reactor. Pet. Sci. Technol. 32 (19), 2275–2282.

Keshavarz, A.R., Rezaei, M., Yaripour, F., 2010. Nanocrystalline gamma-alumina: A highly active catalyst for dimethyl ether synthesis. Powder Technol. 199 (2), 176–179.

Klusáček, K., Schneider, P., 1981. Multicomponent diffusion of gases in a model porous catalyst during methanol dehydration. Chem. Eng. Sci. 36 (3), 517–522.

Klusáček, K., Schneider, P., 1982. Stationary catalytic kinetics via surface concentrations from transient data: Methanol dehydration. Chem. Eng. Sci. 37 (10), 1523–1528.

Li, M. et al, 2021a. Catalytic conversion modeling of methanol in dehydration reactor using Voronoi 3D pore network model. Arabian J. Chem. 14, (9) 103284.

Li, X. et al, 2021b. Increment-oriented online power distribution strategy for multi-stack proton exchange membrane fuel cell systems aimed at collaborative performance enhancement. J. Power Sources 512, 230512.

Li, M. et al, 2021c. Catalytic Conversion Modeling of Methanol in Dehydration Reactor Using Voronoi 3D Pore Network Model. Arabian J. Chem. 103284

Liu, W. et al, 2008. Treatment of CrVI-Containing Mg(OH)2 Nanowaste. Angew. Chem. Int. Ed. 47 (30), 5619–5622.

Lu, W.-Z., Teng, L.-H., Xiao, W.-D., 2004. Simulation and experiment study of dimethyl ether synthesis from syngas in a fluidized-bed reactor. Chem. Eng. Sci. 59 (22), 5455–5464.

Ma, Z.-P. et al, 2022. A dual strategy for synthesizing crystal plane/defect co-modified BiOCl microsphere and photodegradation mechanism insights. J. Colloid Interface Sci. 617, 73–83.

Maloney, J.O., 2008. Perry Chemical Engineers Handbook. The McGraw-Hill Companies, Inc.

Mianmahale, M.A. et al, 2021. Single-bubble EHD behavior into water two-phase flow under electric-field stress and gravitational acceleration using PFM. npj Microgravity 7 (1), 1–11.

Mollavali, M. et al, 2008. Intrinsic Kinetics Study of Dimethyl Ether Synthesis from Methanol on γ-Al2O3 Catalysts. Ind. Eng. Chem. Res. 47 (9), 3265–3273.

Moradi, G. et al, 2010. Intrinsic reaction rate and the effects of operating conditions in dimethyl ether synthesis from methanol dehydration. Korean J. Chem. Eng. 27 (5), 1435–1440.

Moradi, G.R., Ahmadpour, J., Yaripour, F., 2008. Intrinsic kinetics study of LPDME process from syngas over bi-functional catalyst. Chem. Eng. J. 144 (1), 88–95.

Moradi, G.R., Nazari, M., Yaripour, F., 2008. The interaction effects of dehydration function on catalytic performance and properties of hybrid catalysts upon LPDME process. Fuel Process. Technol. 89 (12), 1287–1296.

Mudiyanselage, S.E. et al, 2021. Automated Workers' Ergonomic Risk Assessment in Manual Material Handling Using sEMG Wearable Sensors and Machine Learning. Electronics 10 (20), 2558.

Niknam, B. et al, 2021. Effect of variations internal pressure on cracking radiant coils distortion. Structures 34, 4986–4998.

Ortega, C. et al, 2018. Methanol to dimethyl ether conversion over a ZSM-5 catalyst: Intrinsic kinetic study on an external recycle reactor. Chem. Eng. J. 347, 741–753.

Osman, A.I., Abu-Dahrieh, J.K., 2018. Kinetic investigation of η-Al 2 O 3 catalyst for dimethyl ether production. Catal. Lett. 148 (4), 1236–1245.

Padmanabhan, V., Eastburn, F., 1972. Mechanism of ether formation from alcohols over alumina catalyst. J. Catal. 24 (1), 88–91.

Panasyuk, G. et al, 2015. The thermodynamic properties and role of water contained in dispersed oxides in precursor-boehmite conversion, based on the example of aluminum hydroxide and oxide under hydrothermal conditions in different environments. Russ. J. Phys. Chem. A 89 (4), 592–597.

Pourbavarsad, M.S. et al, 2021. Nitrogen oxidation and carbon removal from high strength nitrogen habitation wastewater with nitrification in membrane aerated biological reactors. J. Environ. Chem. Eng. 9, (5) 106271.

Prausnitz, J.M., Thaler, R.L., Azeredo, E.G., 1988. Molecular Thermodynamics of fluid phase Equilibria. Prentic Hall.

Sahebdelfar, S., Bijani, P.M., Yaripour, F., 2022. Deactivation kinetics of γ-Al2O3 catalyst in methanol dehydration to dimethyl ether. Fuel 310, 122443.

Schiffino, R.S., Merrill, R.P., 1993. A mechanistic study of the methanol dehydration reaction on.gamma.-alumina catalyst. J. Phys. Chem. 97 (24), 6425–6435.

Semelsberger, T.A., Borup, R.L., Greene, H.L., 2006. Dimethyl ether (DME) as an alternative fuel. J. Power Sources 156 (2), 497–511.

Shen, Z. et al, 2022. Effect of K-Modified Blue Coke-Based Activated Carbon on Low Temperature Catalytic Performance of Supported Mn–Ce/Activated Carbon. ACS Omega 7 (10), 8798–8807.

Walas, S.M., 1985. Phase Equilibria in Chemical Engineering. Butterworth-Heinemann.

Wang, Z. et al, 2020. In-situ synthesis of free-standing FeNi-oxyhydroxide nanosheets as a highly efficient electrocatalyst for water oxidation. Chem. Eng. J. 395, 125180.

Wang, X. et al, 2021. Preparing printable bacterial cellulose based gelatin gel to promote in vivo bone regeneration. Carbohydr. Polym. 270, 118342.

Wen, D., Ding, Y., 2006. Heat transfer of gas flow through a packed bed. Chem. Eng. Sci. 61 (11), 3532–3542.

Wu, Y. et al, 2021. Ultra-fast growth of cuprate superconducting films: Dual-phase liquid assisted epitaxy and strong flux pinning. Mater. Today Physics 18, 100400.

Xiong, Q.-M. et al, 2020. Preparation, structure and mechanical properties of Sialon ceramics by transition metal-catalyzed nitriding reaction. Rare Met. 39 (5), 589–596.

Yaripour, F. et al, 2005. Catalytic dehydration of methanol to dimethyl ether (DME) over solid-acid catalysts. Catal. Commun. 6 (2), 147–152.

Yaripour, F. et al, 2009. Catalytic Dehydration of Methanol to Dimethyl Ether Catalyzed by Aluminum Phosphate Catalysts. Energy Fuels 23 (4), 1896–1900.

Yin, G. et al, 2022a. Multiple machine learning models for prediction of CO2 solubility in potassium and sodium based amino acid salt solutions. Arabian J. Chem. 15, (3) 103608.

Yin, G. et al, 2022b. Machine learning method for simulation of adsorption separation: Comparisons of model's performance in predicting equilibrium concentrations. Arabian J. Chem. 15, (3) 103612.

Zhang, L. et al, 2011. Intrinsic kinetics of methanol dehydration over Al2O3 catalyst. Eng. Technol. 59, 1538–1543.